Plasma Physics Reports, Vol. 21, No. 9, 1995, pp. 735 - 742. Translated from Fizika Plazmy, Vol. 21, No. 9, 1995, pp. 775 - 783.

MAGNETIC CONFINEMENT SYSTEMS

Decrease in the Target-Plasma Density during Neutral-Beam Injection into a Tandem Mirror

A. A. Kabantsev, V. G. Sokolov, and S. Yu. Taskaev

Budker Institute of Nuclear Physics, Russian Academy of Sciences, Siberian Division

Received January 11, 1995

Abstract – Experimental results on plasma heating in the AMBAL-Yu device are presented. The phenomenon of the substantial decrease in the jet-plasma-target density during high-energy hydrogen neutral-beam injection is found. A model based on the effect of trapped hot ions on the jet plasma is proposed to explain this phenomenon. The experimental and simulation results are compared.

In previous experiments on plasma heating by neutral beam injection at the AMBAL-Yu device [1], an interesting and unexpected effect was observed: the trapping of high-energy hydrogen atoms by the jet-plasma target accompanied by the production of a hot-ion population results in a substantial decrease in the target plasma density.

1. EXPERIMENTAL LAYOUT

Figure 1 shows the experimental layout of the AMBAL-Yu device. The magnetic adiabatic confinement system AMBAL-Yu is a classical single-stage tandem mirror system with a mirror ratio of 2 and mirror distance of 1 m. A pair of Yin-Yang coils (curve *3* in Fig. 1) form a minimum *B* configuration of magnetic field with quadrupole symmetry. In the midplane, the magnetic field increases by 7% from the plasma center towards the boundary (radius 10 cm) to provide MHD-stability conditions. The magnetic field is 0.65 T in the center of the device.

The hot-ion plasma was produced due to high-energy neutral-beam trapping by the jet-plasma target. This plasma jet was produced by the arc source with a slot discharge channel (curve *1* in Fig 1) described in [2]. The arc was located at the end of the mirror-device upstream from the magnetic plug at a distance of 1.8 m from the trap center. The plasma jet was injected along the magnetic field lines. It was subsonic upstream and supersonic downstream from the plug. The plasma-target peak density was about 2.5×10^{14} cm^{-3} and the electron and ion temperature was 10 eV. The beam of 17 keV hydrogen atoms with a flow current (expressed in electric current units) up to 160 A was injected perpendicularly to the axis, the injection time being 200 μs [3]. The target plasma (with average thickness in the injection region of order 10^{15} cm^{-2}), presumably, was able to trap 50% of the beam atoms. Ionization of the injected atoms by the plasma electrons and ions, as well as charge-exchange (when the plasma ion is only replaced with the high-energy ion), produced a hot-ion population with average energy of 6 keV and with density up to 1.1×10^{13} cm^{-3} in the plasma volume about 3 l [4]. The energy confinement time of the hot ions, determined by their slowing down due to ion-electron collisions, was ≈25 μs. The confinement time of the plasma ions, determined by the loss-cone scattering, was ≈70 μs (with allowance for slowing down due to ion-electron collisions). During injection, the electron temperature increased to 25 eV and the target plasma density decreased by a factor of 2.5.

A variety of diagnostics was used to determine the plasma parameters. The following is a representative list of diagnostics used in the measurements. The plasma dimension, density, and potential, as well as the electron and ion temperatures in different positions in the chamber, were determined from the volt-ampere characteristics of Langmuir probes. We determined the plasma density per unit length by measuring the losses of the diagnostic and heating neutral beams. To measure the ion temperature, we used a cesium low-energy atom analyzer [5] recording the charge-exchange spectra of atoms from the center of the device, and the magnetic and electrostatic multigrid analyzers (curve *4* in Fig. 1) recording the energy spectrum of ions escaping from the device along the longitudinal axis. We determined the electron temperature by comparing the losses of the diagnostic high-energy hydrogen, argon, and helium atom beams, and on the basis of the measurements of hot-ion slowing-down rate by means of the 5-channel electrostatic analyzer of charge-exchange particle energy spectra.

2. EXPERIMENTAL RESULTS

The experiment shows that the neutral-beam injection results in the substantial decrease (by a factor of 2.5) of the target plasma density. The time dependence of

1063-780X/95/2109-0735$10.00 © 1995 МАИК Наука / Interperiodica Publishing

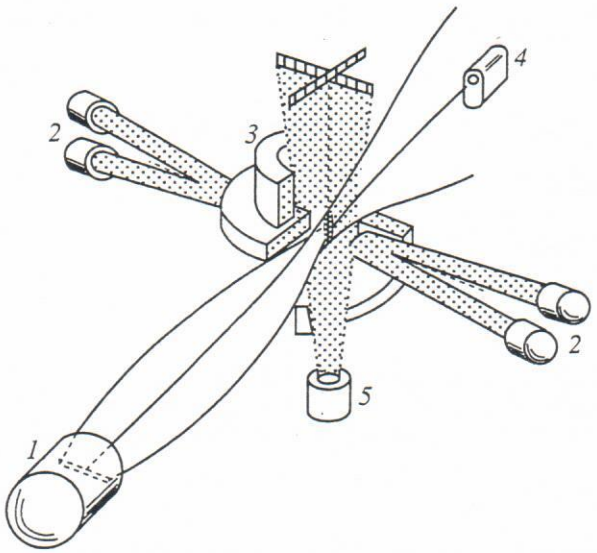

Fig. 1. Schematic of the AMBAL-Yu device: (*1*) gas-discharge source with solenoid, (*2*) hydrogen atom-beam injectors, (*3*) magnetic-field coils, (*4*) diagnostic analyzers in the widener, and (*5*) diagnostic atom-beam injector.

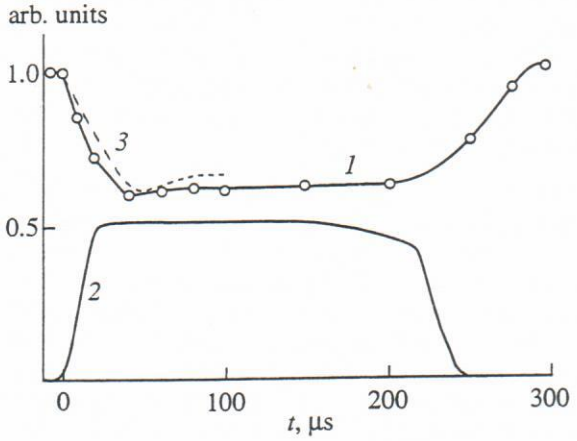

Fig. 2. Time dependences of plasma density at the device center (*1*), injection current (*2*), and calculated plasma density (*3*).

the plasma density at the center of the device is shown in Fig. 2.[1] The jet dimensions change only slightly, if at all. Between the injection region and the input plug (on the plasma-source side), a shock wave propagating upstream is observed. The analyzers (curve *4* in Fig. 1) and bolometer, which are located at the plasma receiver, detect a substantial increase in the ion energy (Fig. 3) and heat flux. The ion-flux time behavior is as follows: ≈30 μs after the injection start-up, the ion flux sharply increases; then it falls off to a level lower than the initial one and returns to the initial level in some time before the end of the injection pulse. The floating potential of the probes does not change.

At the same time, the jet-plasma parameters measured with the probe in the upstream region from the input plug do not change noticeably during the injection. Plasma losses in the transverse direction do not explain the drop-density effect either. The plasma source operation (discharge voltage and current) do not change. Plasma ion-cyclotron radiation does not grow. Since the injected beams are symmetrical with respect to the axis, the momentum transfer from the neutral beams to the target plasma does not play an important role, and even the artificially produced asymmetrical injection does not result in qualitative effects (including the hydrodynamic instability).

3. NUMERICAL MODEL

Consider a plasma stream within the framework of magnetic hydrodynamics [6, 7].

A plasma component is characterized by the following macroscopic parameters: density n, temperature T, and flow velocity u. The set of equations describing the macroscopic parameters consists of the continuity equation and the momentum and energy transfer equations.

In the framework of single-fluid magnetic hydrodynamics, neglecting viscosity, the analysis of the one-dimensional, steady adiabatic ion flow moving along the homogeneous axial-magnetic-field lines shows that the external heating results in the acceleration of the subsonic flow and, consequently, in the decrease of the plasma density. For the theory and experiment to be in agreement, a heating power of one hundred kilowatts is necessary. However, the direct collisional energy transfer from hot ions to plasma ions enables the heating power to be less than ten kilowatts. Thus, this simplified model cannot explain the ion-heating mechanism.

Below, we will consider the plasma flow moving along the inhomogeneous magnetic field lines within the framework of two-fluid magnetic hydrodynamics. We will seek a time-dependent solution for the plasma-jet parameters on the axis, provided that the high-energy ion population (with density n_{hot}, average energy E_{hot}, and average longitudinal pressure $p_{hot\|}$) appears in the local volume.

We assume that the fully ionized plasma contains only protons and electrons.

We suppose that the ion flow velocity is equal to electron flow velocity. Such an equality is experimentally proven by measurement of the electron current at the end-face surfaces of the plasma receiver [8].

A substantial target-plasma density drop takes place when the hot-ion density is only about 1% of the jet-plasma density. Hence, we assume plasma quasineutrality approximation $n_e = n_i$ everywhere in the plasma volume including in the hot-ion region. As estimates show, this assumption does not noticeably change the

[1] In Fig. 2, the numerical results are also shown. Below, we consider this numerical model. Some experimental results are presented in the section where the dependences calculated numerically are compared with the measured ones.

calculated jet-plasma parameters. Below, n (without index) will represent both the jet-electron and ion densities.

We assume $\partial \mathbf{B}/\partial t = 0$, neglecting the magnetic field variation which appears due to the presence of plasma. The decrease in the magnetic field value does not exceed 2% with respect to the vacuum's magnetic field because of the small value of β for both the jet-plasma and hot-ion components. Henceforth, we set B equal to the value of the vacuum field produced by the coils and plasma-source solenoid.

We use a coordinate system with the z-axis aligned with the magnetic field lines. We write the velocity vector as $\mathbf{u} = u\mathbf{B}/B$, so that $\mathbf{u}$ is directed along the z-axis.

We neglect the electron inertia. For the strong magnetic field ($\omega\tau \gg 1$, where ω and τ are the cyclotron frequency and collisional time, respectively), we retain a single component π_{izz} of the viscosity stress tensor components $\pi_{z\alpha}$, neglecting the terms of order $(\omega\tau)^{-1}$ and $(\omega\tau)^{-2}$.

The plasma source is located at a boundary. There are no internal sources producing electrons and ions inside the plasma volume.

The set of equations including the continuity, motion, and heat flux equations can be written in the following form:

$$\frac{\partial n}{\partial t} + B\frac{\partial}{\partial z}\left(\frac{nu}{B}\right) = 0, \tag{1}$$

$$Mn\left(\frac{\partial u}{\partial t} + u\frac{\partial u}{\partial z}\right) = -\frac{\partial p}{\partial z} - \frac{\partial \pi_{izz}}{\partial z}, \tag{2}$$

$$\frac{\partial}{\partial t}\left(\frac{Mn}{2}u^2 + \frac{3}{2}p_i\right) + B\frac{\partial}{\partial z}\left\{\frac{1}{B}\left(\left(\frac{Mn}{2}u^2 + \frac{5}{2}p_i + \pi_{izz}\right)u - \chi_{\parallel}^{i}\frac{\partial T_i}{\partial z}\right)\right\} = Q_i, \tag{3}$$

$$\frac{\partial}{\partial t}\left(\frac{3}{2}p_e\right) + B\frac{\partial}{\partial z}\left\{\frac{1}{B}\left(\frac{5}{2}p_e u - \chi_{\parallel}^{e}\frac{\partial T_e}{\partial z}\right)\right\} = Q_e. \tag{4}$$

Here, M and m are the proton and electron mass, respectively.

Pressure is $p = p_i + p_e$, where $p_i = n_i T_i$ and $p_e = n_e T_e$.

The viscosity stress tensor component is written as

$$\pi_{izz} = -\eta_0^i W_{zz}, \quad \eta_0^i = 0.96 n_i T_i \tau_i,$$

$$W_{zz} = 2\frac{\partial u}{\partial z} - \frac{2}{3}B\frac{\partial}{\partial z}\left(\frac{u}{B}\right),$$

where τ_i is the ion collisional time.

Heat fluxes are expressed by the following formulas:

$$q_i = -\chi_{\parallel}^{i}\nabla_{\parallel}T_i \text{ and } q_e = -\chi_{\parallel}^{e}\nabla_{\parallel}T_e,$$

where χ is the thermal conductivity [6].

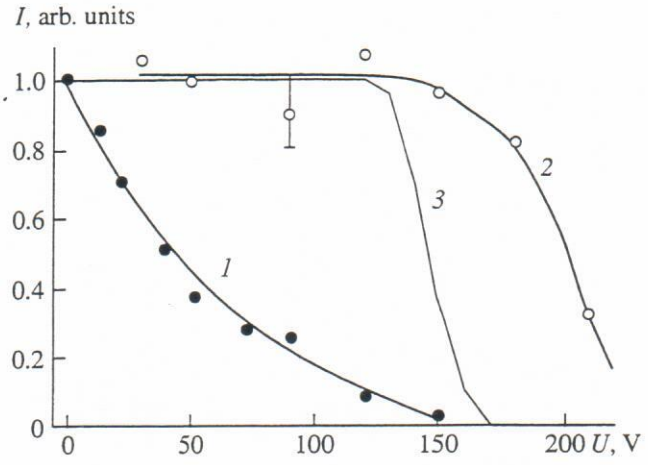

Fig. 3. Dependence of the end-face electrostatic analyzer current on the retarding voltage: (*1*) before the neutral-beam injection, (*2*) during injection, and (*3*) calculation for $n_{\text{hot}} = 4 \times 10^{12}$ cm^{-3}.

On the right-hand side of the energy-transfer equations (3) and (4), the Q-terms denote the heat sources:

$$Q = Q_{ei} + Q_{\text{hot}} + Q_{FR}.$$

Here, Q_{ei} is the heat source due to electron–ion collisions:

$$Q_{ei}^{i} = -Q_{ei}^{e} = \frac{3m}{M}\frac{n}{\tau_e}(T_e - T_i),$$

where τ_e is electron collisional time.

Q_{FR} is the heat source due to the work done by the electron pressure force:

$$Q_{FR}^{i} = -Q_{FR}^{e} = -u\frac{\partial p_e}{\partial z}.$$

The electron and ion heat sources due to collisions with hot ions are

$$Q_{\text{hot}}^{e} = n_{\text{hot}}\frac{E_{\text{hot}}}{\tau_E^e}, \quad Q_{\text{hot}}^{i} = n_{\text{hot}}\frac{E_{\text{hot}}}{\tau_E^i},$$

where τ_E^e and τ_E^i are the times of the collisional energy transfer between the hot ions and the jet electrons and ions, respectively. In our case, this time can be represented in a sufficiently simple form [9]. When $mE_{\text{hot}} \ll MT_e$, τ_E^e is expressed as the ion slowing-down time due to collisions with electrons: $\tau_E^e = \tau_E^e(E_{\text{hot}}) \approx \tau_{dr}$. When $E_{\text{hot}} \gg T_i$, τ_E^i is determined by the ion–ion collisional time: $\tau_E^i = 0.5\tau_1^{ii}$.

This set of equations needs an additional explanation.

We neglect the change of both the electrons and ion momentum due to collisions with the hot ions because of the high value of hot-ion longitudinal pressure (the averaged longitudinal temperature $T_{\text{hot}\parallel} \sim 500$ eV).

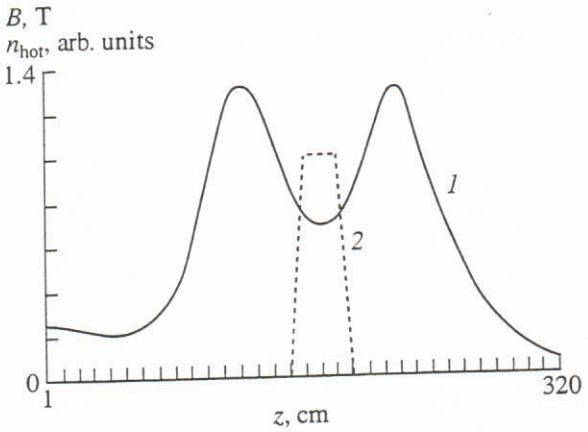

Fig. 4. Magnetic-field (*1*) and hot-ion density (*2*) distributions along the *z*-axis used in calculations.

If we define the change of the particle momentum $\mathbf{p}_\alpha$ during decay time τ_p^α as $d\mathbf{p}_\alpha/dt = -M\mathbf{u}/\tau_p^\alpha$ [9], then for the typical parameters of the problem, we obtain an estimate $\tau_p^i \sim \tau_p^e \sim 10$ ms. Since the plasma jet flows through the hot-ion region during 10 μs, the proton and electron momentums change due to the electron–ion collisions.

We write the energy transfer equation in the general form [6]:

$$\frac{\partial}{\partial t}\left(\frac{Mn}{2}u^2 + \frac{3}{2}p\right) + B\frac{\partial}{\partial z}\left\{\frac{1}{B}\left(\left(\frac{Mn}{2}u^2 + \frac{5}{2}p\right)u + \pi_{\beta z}u_\beta + q\right)\right\} = n\mathbf{F}\mathbf{u} + \mathbf{R}\mathbf{u} + Q,$$

where the first and second terms on the right-hand side of the equation account for the work done, respectively, by the "smoothed" macroscopic electrical force $\mathbf{F}_\alpha = e_\alpha\mathbf{E}$ and the fast-fluctuating collisional microforces arising at short distances between particles; and the third term accounts for the heating of the particles of a given kind due to collisions with other particles.

As follows from the electron motion equation [6, p. 191], the macroscopic and collisional forces are in equilibrium with the electron-pressure gradient. Then, the heating of the electron and ion components due to the work done by these forces is expressed as Q_{FR} (see the above formula).

The initial conditions describe the plasma-jet flow in the absence of the hot ions.

In the case of steady plasma flux emerging from the plasma source with fixed electron and ion temperatures, we write the boundary conditions near the plasma source as follows: $T_e = \text{const}$, $T_i = \text{const}$, $nu = \text{const}$, and $\partial n/\partial z = 0$.

The other boundary is in the widener. Here, the flow is supersonic and the particle mean-free-path is sufficiently large. Here, the hydrodynamics approach is applicable. A material wall is far from this boundary. Allowing for heat to transfer freely through this "virtual" boundary, we define the following boundary conditions: $\partial^2 T_e/\partial z^2 = 0$, $\partial^2 T_i/\partial z^2 = 0$, and $\partial^2 u/\partial z^2 = 0$.

The purpose of our study is to examine the changes in the plasma flow parameters produced by the hot-ion population.

The set of partial differential equations to be solved contains a first-order equation of the hyperbolic type (the continuity equation) and three second-order equations of the parabolic type. As an approximation, a numerical method is used to solve the set of partial differential equations, i.e., the grid method.

We approximate the spatial derivatives in the second-order equations with the three-point difference formula of second-order accuracy. In the continuity equation, we use the two-point difference formula of first-order accuracy. We use the uniform grid with 320 points and step $\Delta z = 1$ cm. For the time derivative Δt, we use a simple formula of first-order accuracy.

As a result, we obtain an explicit system of difference schemes that are solvable. The stability analysis of the difference schemes [10 - 13] shows that all difference schemes are stable when the appropriate steps Δz and Δt are chosen. The difference schemes are absolute approximations for differential equations. The approximability and stability of the difference scheme is a necessary and sufficient condition for the difference solution to converge to a precise solution of the differential equations at $\Delta t, \Delta z \longrightarrow 0$.

We solve a mixed (space-time) problem. We seek a solution of the given set of equations in the rectangle ($1 \le z \le 320$ cm, $0 \le t \le 100$ μs) that satisfies the initial and boundary conditions.

The left boundary ($z = 1$) is the exit section of the gas discharge source. The right boundary ($z = 320$) is in the low magnetic-field region of the widener. The boundary conditions are given by the following relations for the left boundary: $T_e(1, t) = T_e(1, 0)$, $T_i(1, t) = T_i(1, 0)$, $n(1, t) = n(2, t)$, and $n(1, t)u(1, t) = n(1, 0)u(1, 0)$. For the right boundary, we write $T_i(320, t) = 2T_i(319, t) - T_i(318, t)$ and analogous relations.

We use the steady-state solution of the Cauchy problem for the above set of differential equations with eliminated terms describing the hot ions as the initial condition for the mixed problem. To define this initial condition, the functions $n(z)$, $u(z)$, $T_e(z)$, and $T_i(z)$ are to be found, providing the following left-boundary conditions: $T_e(1) = 10$ eV, $T_i(1) = 10$ eV, $n(1) = 2 \times 10^{14}$ cm^{-3}, and $u(1) = 0.61 \times 10^6$ cm/s. The first three parameters are typical jet-plasma parameters measured in the experiment. We fitted the boundary flow-velocity value so that the flow velocity was close to the ion acoustic speed in the magnetic plug regions. It is necessary to provide the transition from subsonic to supersonic flow in the exit plug region, as it occurs in the experiment.

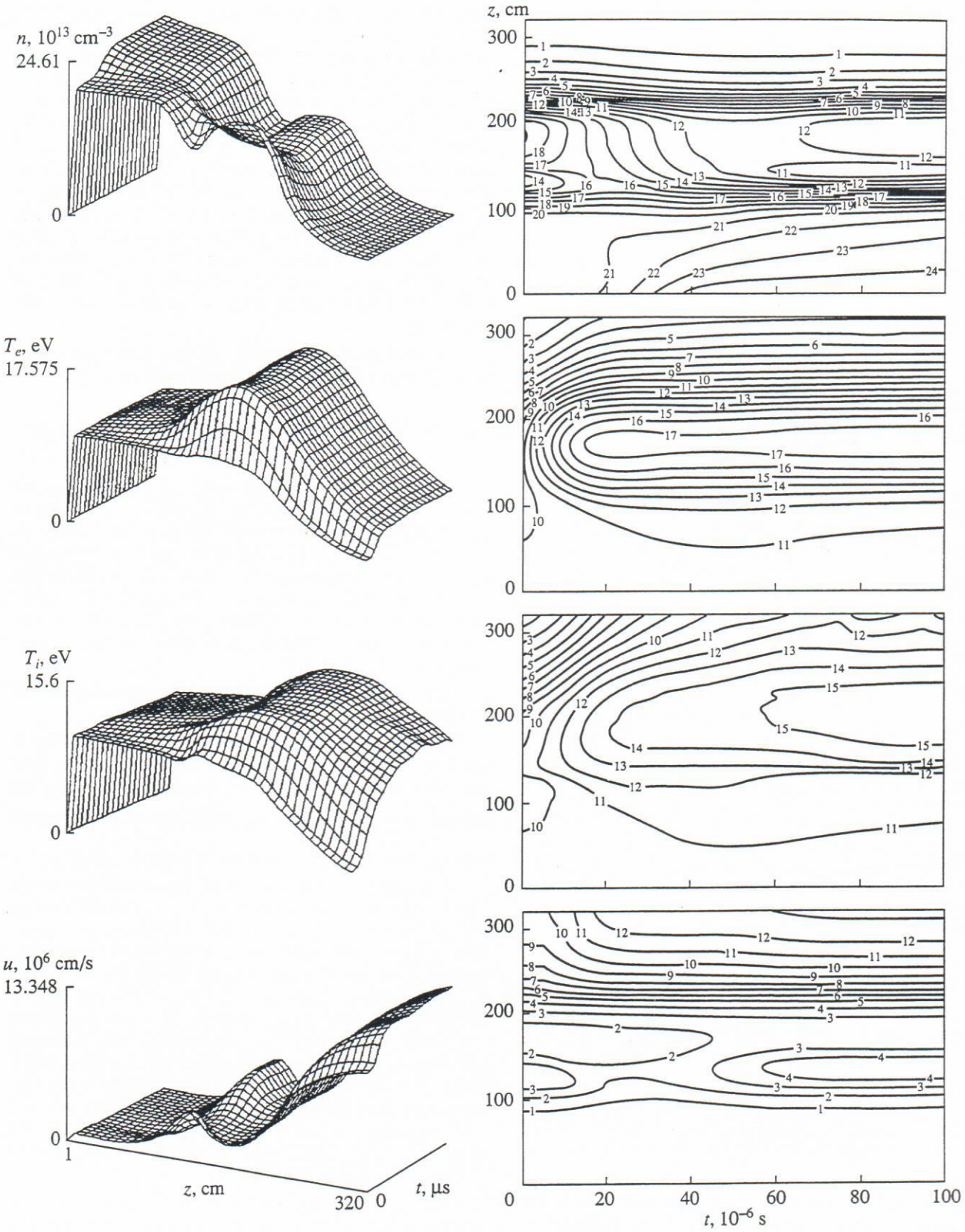

Fig. 5. The calculated isometric profiles (on the left) and isoline graphs (on the right) of the evolution of spatial distributions of n, T_e, T_i, and u.

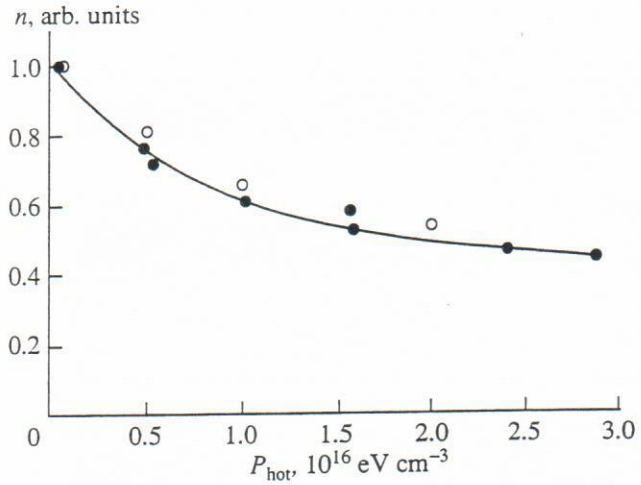

Fig. 6. Dependence of the plasma density at the trap center on the hot-ion energy density (dark spots – experiment, bright spots – calculation).

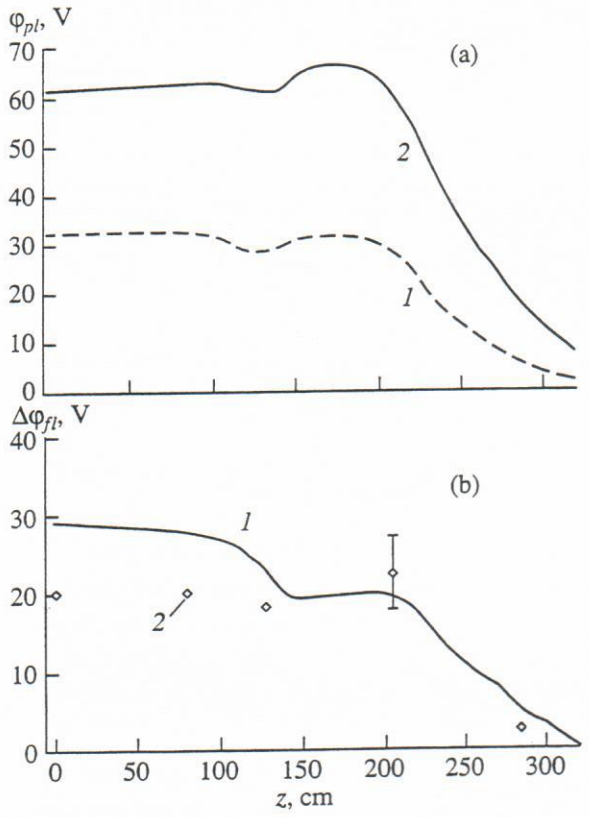

Fig. 7. (a) Plasma potential distribution at $t = 0$ μs (*1*) and $t = 100$ μs (2). (b) The variations of the probe floating potential due to hot ions: (*1*) calculation and (2) experiment.

Rognlien and Brengle [14] pointed out the possibility of a similar regime when a plasma flows through two identical magnetic plugs. We simplified the set of equations for the steady-state problem to an explicit form and solved it in two intervals. We seek a solution of the Cauchy problem, which satisfies the following conditions: the plasma flow is subsonic in the interval (1; 220); it is close to sonic in the plugs; and it is supersonic in the interval (220; 320). The point $z = 220$ corresponds to the exit plug position. At this point, the solutions for the second interval were set to equal those for the first interval. The exception was for the flow velocity at the second interval which at $z = 220$ was chosen to be equal to the acoustic speed that was somewhat higher than the flow velocity given by the solution for the first interval at this point. Then, the obtained solutions were applied as the initial solution for the time-dependent problem (with the hot-ion terms still excluded). Finally, the convergent solution of the time-dependent problem was used as the initial condition for the problem under consideration.

The choice of the model, difference scheme, and problem specification is discussed in detail in [15].

4. NUMERICAL RESULTS AND COMPARISON WITH EXPERIMENT

Figure 4 shows the magnetic field and the hot-ion density distribution along the z-axis that were used in the calculations. We assumed the hot-ion density to grow linearly during 10 μs up to 2×10^{12} cm^{-3} and then to be constant in time. Note that the numerical results for the hot-ion densities of 1×10^{12} and 4×10^{12} cm^{-3} do not differ qualitatively; that is why they are presented only in Figs. 3 and 6 with special comments. The hot-ion energy was $E_{hot} = 5$ keV.

Figure 5 shows the solution of the time-dependent problem.

The hydrodynamic approximation is applicable in our study because the particle mean-free-path is less than the local scale length of the magnetic-field variation defined as $\left|\frac{B}{dB/dz}\right|$ and the collisional time is greater than the time scale of the plasma parameter variations.

Note that we carried out calculations with the modified conditions at the right boundary in the widener as well: $\partial T_e/\partial z = 0$, $\partial T_i/\partial z = 0$, and $\partial u/\partial z = 0$. Such conditions mean that both thermal-conductivity heat flux through the boundary and viscosity stress tensor vanish at the boundary. This results only in the noticeable change of the plasma parameters near this boundary (T_e, T_i, and u increase while n decreases). With different boundary conditions, the solutions differ within 0.4% in the interval (1; 220). Presumably, the right-boundary conditions only slightly affect the solution because near this boundary the flow is supersonic, the heat flux due to the thermal conductivity is relatively small, and the viscosity has practically no effect.

Figures 2, 3, 6, and 7 show the experimental dependences compared with those calculated: the plasma density at the center of the device as a function of time and the hot-ion energy density, the end-face electrostatic energy analyzer current as a function of the retarding voltage, and the plasma potential profiles.

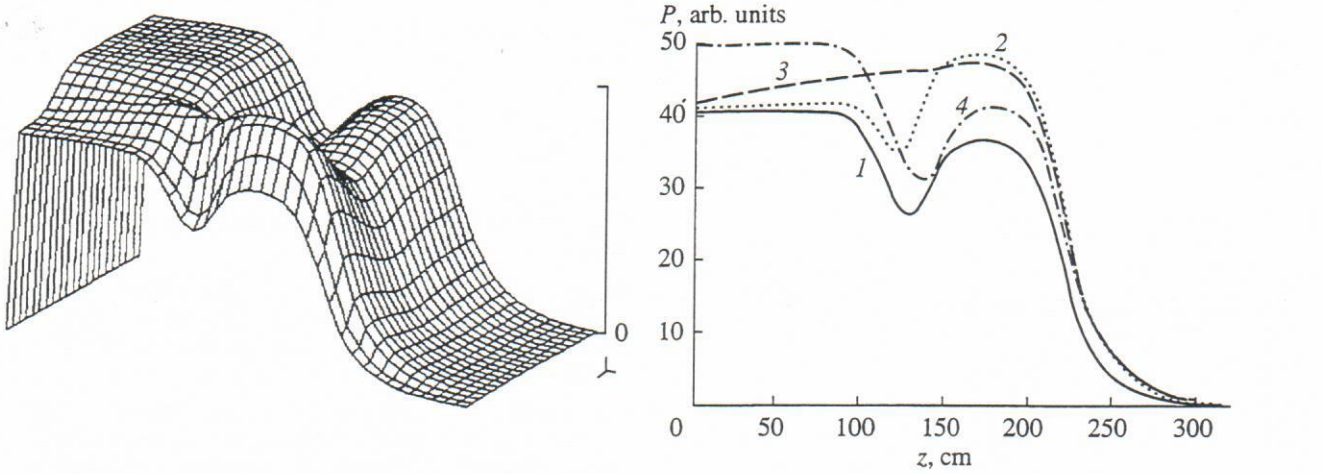

Fig. 8. The calculated isometrical profiles (on the left) of the plasma pressure (coordinates are the same as in Fig. 5) and the pressure profiles at different times (on the right) [(*1*) 0 μs, (*2*) 10 μs, (*3*) 20 μs, and (*4*) 100 μs].

The calculation results agree well with the probe and bolometer measurement data. In the transport region (z = 80 cm), the probe indicates no noticeable change in the plasma density and electron temperature. The bolometer current increases by a factor of 4 during injection, the bolometer being located next to the end-face electrostatic energy analyzer in the widener. As for the plasma density distribution along the z-axis, we observed a shock wave moving from the injection region toward the source (Fig. 5).

This comparison shows that the simulation results agree well with the experimental results.

5. DISCUSSION

During the neutral-beam injection into the tandem mirror filled in advance with the jet-target plasma, the hot-ion population appears after a short time (of the order 20 μs). The hot ions, colliding with electrons cause a fast heating of the electrons. The plasma pressure substantially increases in the local region (Fig. 8). The plasma flow slows down and the plasma density grows in the upstream region. Because of the electron heating due to the high electron thermal conductivity and ion heating due to electron–ion collisions, the high-pressure region extends toward the source. This process is associated with the shock wave. In the steady state, the plasma pressure grows in the entire transport region (from the source to the input plug). When the plasma flows down from the hot-ion region, the density decreases due to both the initial decrease in the plasma flux itself and the flow acceleration due to the increased pressure gradient. Although the plasma temperature increases here, the pressure increases to a smaller degree. In the steady-state regime, the plasma flux is restored to its initial value. However, the plasma flow accelerates due to the increased pressure gradient and, consequently, the target-plasma density decreases.

In summary, we find that the target-plasma density decrease is due to the following effects of the hot ions on the plasma flow: (1) the plasma flux decrease at the initial stage because of plasma slowing-down upstream from the injection region and (2) the flow velocity increase at the steady state.

The steady-state energy balance was calculated. The main part of the hot-ion power[2] (of the order 230 kW) transfers to electrons and only about 3 kW transfers to ions. Because of the high electron thermal conductivity, the input energy is carried away in equal shares upstream and downstream from the hot-ion region. In the upstream region, this power is spent on electron and ion heating due to electron–ion collisions and through the work done by the thermal electromotive force; about 30 kW of power is lost through the end-face. In the downstream region, the power is spent on ion acceleration by the electric field. Ion heating due to the work done by the forces (electrical field and, partially, thermoforce) $Q_{FR} \approx 160$ kW plays an important role in the energy transport processes as well as in electron heating by hot ions and in electron thermal conductivity. The typical values of the other power terms are as follows: $Q^i_{visc} \approx \frac{3}{4}\eta^i_0 W^2_{zz} \approx 30$ kW and $Q_{ei} \approx 16$ kW. Figure 9 shows the energy flux. The input power is lost mainly through the macroscopic flux of the ion kinetic energy. The ions are accelerated by the electric field which is regenerated by the power supply due to the electron thermal conductivity. In our experiments, the energy loss through the left boundary does not play an important role in the hot-ion accumulation process. This explains the failure to increase the hot-ion density by decreasing thermal conductivity. Neither the change

[2] Below, the energy flux values are averaged over the entire volume of the plasma jet, the midplane area being 70 cm^2. This generalization is valid because of the small viscosity effect.

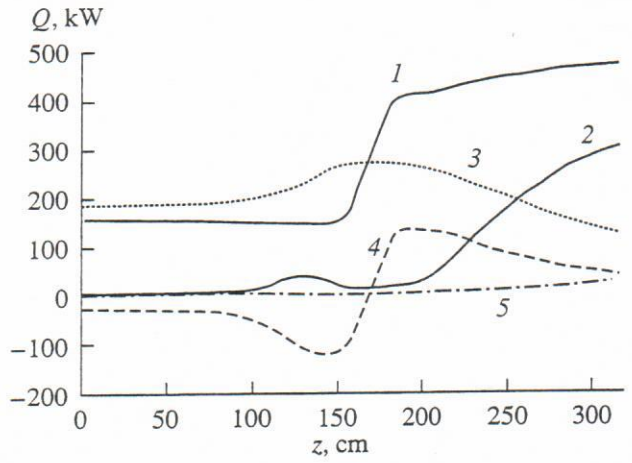

Fig. 9. Total energy flux distribution along the z-axis at t = 100 μs (*1*) and the flux component distributions: kinetic energy flux (*2*), internal energy and work done by pressure (in one curve) (*3*), electron (*4*), and ion (*5*) heat flux. The heat flux due to viscosity is not shown, because of its low value.

in the current direction in the plasma-source solenoid (which causes a cusp geometry of magnetic filed lines) nor the fast termination of the source discharge resulted in a hot-ion density increase.

6. CONCLUSION

An interesting and unexpected phenomenon was observed and studied in the AMBAL-Yu device: the high-energy hydrogen atom beam injection into the device results in a substantial decrease of the jet-plasma-target density.

We considered the hot-ion population effect on the plasma jet flowing along the inhomogeneous magnetic field lines within the framework of two-fluid magnetic hydrodynamics. We solved the time-dependent problem by using numerical methods. We compared the numerical results with the experiment. They are in acceptable agreement.

Based on the numerical results, we explained the main features of the phenomenon involved.

ACKNOWLEDGMENTS

The authors gratefully acknowledge V.E. Chuprianov for his assistance in the experiments in the AMBAL-Yu device and G.I. Dimov for his support of this work.

REFERENCES

1. Bender, E.D., Chupriyanov, V.E., Dimov, G.I., *et al.*, *Proc. Workshop Held at Villa Monastero*, Varenna (Italy), October 15 - 24, 1990, p. 157.
2. Dimov, G.I., Kabantsev, A.A., and Taskaev, S.Yu., *Voprosy Atomnoi Nauki i Tekhniki, Ser.: Termoyadernyi Sintez* (Problems of Atomic Science and Technology), (Nuclear Fusion), 1989, vol. 3, p. 58.
3. Davydenko, V.I., Roslyakov, G.V., and Savkin, V.Ya., *Voprosy Atomnoi Nauki i Tekhniki, Ser.: Termoyadernyi Sintez* (Problems of Atomic Science and Technology), (Nuclear Fusion), 1983, vol. 2, p. 67.
4. Gilev, E.A., Dimov, G.I., Kabantsev, *et al.*, *Proc. Int. Conf. on Open Plasma Confinement Systems for Fusion*, Novosibirsk (Russia), June 14 - 18, 1993, p. 485.
5. Dudnikov, V.G., Taskaev, S.Yu., and Fiksel', G.I., *Fiz. Plasmy*, 1994, vol. 20, p. 199 [*Sov. J. Plasma Phys.* (Engl. Transl.), vol. 20, p. 183].
6. Braginskii, S.I., *Voprosy Teorii Plazmy* (Problems of Plasma Theory), Moscow: Atomizdat, 1963, vol. 1, p. 183.
7. Dawson, J.M. and Uman, M., *Nucl. Fusion*, 1965, vol. 5, p. 242.
8. Kabantsev, A.A., Karliner, V.M., Sokolov, V.G., *et al.*, *Preprint of Inst. of Nuclear Physics, USSR Acad. Sci., Sib. Div.*, Novosibirsk, 1989, no. 46.
9. Trubnikov, A., *Voprosy Teorii Plazmy* (Problems of Plasma Theory), Moscow: Atomizdat, 1963, vol. 1, p. 98.
10. Berezin, I.S. and Zhidkov, N.P., *Metody Vychislenii* (Methods of Calculations), Moscow: Fizmatgiz, 1959, p. 410.
11. Berezin, I.S. and Fedoruk, M.P., *Modelirovanie Nestatsionarnych Plazmennykh Protsessov* (Non-Steady Plasma Process Simulation), Novosibirsk: Nauka, 1993, p. 356.
12. Samarskii, A.A. and Popov, Yu.P., *Raznostnye Skhemy Gazovoi Dinamiki* (Difference Schemes for Gas Dynamics), Moscow: Nauka, 1975, p. 351.
13. Kunin, S., *Vychislitel'naya Fizika* (Calculations in Physics), Moscow: Mir, 1992, p. 513.
14. Rognlien, T.D. and Brengle, T.A., *Phys. Fluids*, 1981, vol. 24, p. 871.
15. Taskaev, S.Yu., *Preprint of Inst. of Nuclear Physics, USSR Acad. Sci., Sib. Div.*, Novosibirsk, 1994, no. 47.